

Controllable electron spin dephasing due to phonon state distinguishability in a coupled quantum dot system

Michał Gawęlczyk,^{1,2,*} Mateusz Krzykowski,¹ Krzysztof Gawarecki,¹ and Paweł Machnikowski¹

¹*Department of Theoretical Physics, Faculty of Fundamental Problems of Technology, Wrocław University of Science and Technology, 50-370 Wrocław, Poland*

²*Department of Experimental Physics, Faculty of Fundamental Problems of Technology, Wrocław University of Science and Technology, 50-370 Wrocław, Poland*

We predict a spin pure dephasing channel in electron relaxation between states with unequal Zeeman splittings, exemplified by a spin-preserving electron tunneling between quantum dots in a magnetic field. The dephasing is caused by a mismatch in electron g -factors in the dots leading to distinguishability of phonons emitted during tunneling with opposite spins. Combining multiband $\mathbf{k}\cdot\mathbf{p}$ modeling and dynamical simulations via a Master equation we show that this fundamental effect of spin measurement effected by the phonon bath may be widely controlled by the size and composition of the dots or on demand, via tuning of external fields. By comparing the numerically simulated degree of dephasing with the predictions of general theory based on distinguishability of environment states, we show that the proposed mechanism is the dominant phonon-related spin dephasing channel and may limit spin coherence time in tunnel-coupled structures at cryogenic temperatures.

I. INTRODUCTION

Quantum systems, distinguished from their classical counterparts by coherent superpositions of states, may lose this quantum nature via pure dephasing processes due to the build-up of correlations with the environment. The resulting emergence of classicality is connected with a transfer of the which-way information, the name of which comes from the analogy with double-slit interference experiments.^{1,2} Demonstrations of such processes in various physical systems attract persistent attention.³⁻⁶ On the other hand, dephasing processes are critically destructive for coherent control of quantum states aimed at applications in spintronics⁷⁻¹⁰ and quantum information processing,^{11,12} where coherent superpositions of states, *e.g.*, single spins in quantum dots (QDs),¹³⁻¹⁷ can be used for computations beyond the classical schemes.^{18,19}

Recently, we have found in a simple model of carrier tunneling in a system of coupled QDs²⁰ that spin-preserving orbital relaxation can be accompanied by spin pure dephasing if the environment response to the relaxation process depends on the spin state. This effect does not rely on any direct or spin-mixing-induced spin-environment interaction and is exclusively due to a misfit between electron g -factors, and hence Zeeman splittings, in the two QDs. The resulting unequal tunneling transition energies for the two spin states cause dephasing that may be interpreted in terms of which-way information: the state of the phonon bath after tunneling depends on the electron spin state. In this way, the bath “measures” the spin state via dissipated energy. Although this process takes place during tunneling (orbital relaxation), it does not lead to spin relaxation, and hence constitutes a pure dephasing on the spin subsystem. While spins in QDs offer long life times²¹ and, under certain conditions, coherence times,²² this dephasing channel may limit the fidelity of spin states in tunnel-coupled structures.²³

Here, we present accurate modeling of quantum states and dynamical simulations of spin pure dephasing that accompanies tunneling of electrons in double QD (DQD) systems. We focus on the controllability of the degree of dephasing: it depends on the spectral overlap of emitted phonon wave packets, which is determined by tunneling times and the Zeeman splittings mismatch only. We derive this fully general relationship explicitly from the Weisskopf-Wigner theory of spontaneous emission and make a quantitative connection between the distinguishability of phonons and the information about the spin state that leaks to the environment during tunneling.

Comparing these calculations with the results of simulations containing all leading-order phonon-driven and spin-orbit effects, we determine the investigated channel to be the dominant phonon-related spin dephasing mechanism in the system under consideration. Its qualitative understanding and quantitative characterization allow us to propose ways of controlling the dephasing magnitude via appropriate sample design or tuning of external fields, the latter yielding feasible and promising methods of real-time control. This may lead to double-slit-like experiments with a continuously controlled level of “observation”, but it may also be relevant for operations like spin-state transfer via non-resonant tunneling and spin-manipulation protocols in tunnel-coupled nanostructures. The dephasing mechanism itself is generic and should be manifested in transitions between states with different Zeeman splittings in any atomic, molecular or solid-state system.

The paper is organized as follows. In Sec. II, we define the system under study and present its theoretical modeling including multiband calculation of electron states and dynamical simulations. Next, in Sec. III, we derive the general expression for the spin coherence preserved after orbital relaxation. The results are presented in Sec. IV, where we also propose methods of dephasing control. Following this, in Sec. V, we investigate the additional dephasing that arises at finite temperatures. Finally, we conclude the paper in Sec. VI. In the [Appendix](#), we give detailed information about numerically modeled structures.

* michal.gawelczyk@pwr.edu.pl

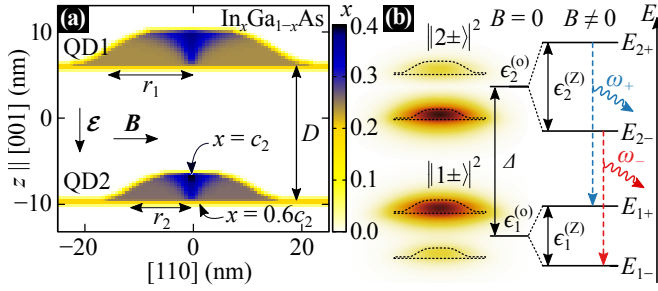


FIG. 1. (a) Exemplary structure material composition. (b) Projection of electron density in the two orbital states and the diagram of energy levels. Dashed arrows mark tunneling transitions.

II. SYSTEM AND ITS THEORETICAL MODELING

We begin by describing the DQD system under investigation and methods used for its theoretical modeling. This is followed by a showcase of spin evolution for exemplary structures.

We consider two vertically stacked, axially symmetric, coaxial, dome-shaped $\text{In}_x\text{Ga}_{1-x}\text{As}$ QDs with a trumpet-shaped gradient of intradot In content^{24,25} (from $x = 0.6c_i$ at the base to c_i at the top of QDi, $i = 1, 2$), base radii r_i and height $h_i = r_i/3$, separated by the distance $D = 15.6$ nm [see Fig. 1(a) for an exemplary material profile]. The structural parameters of QD2 are fixed: $r_2 = 12$ nm and $c_2 = 0.43$, while for QD1 they are varied: $r_1 = 10.7$ -16.1 nm and $c_1 = 0.35$ -0.5, which mainly alters the electron g -factor mismatch between QDs, Δg , but also, to a small extent, affects the phonon-assisted tunneling rates. In total, 50 structures were modeled to cover the r_1 - c_1 plane with a grid (see the Appendix). In Table I, we present structural and calculated parameters of structures serving as exemplary throughout the paper, which are selected to represent various regimes of behavior.

Electron wave functions are calculated within the 8-band envelope-function $\mathbf{k}\cdot\mathbf{p}$ theory,^{26–28} including spin-orbit effects, electric and magnetic fields,²⁹ strain,^{30,31} and piezoelectric field up to second-order terms^{32–34} (see Ref. [35] for details of the model, numerical methods, and all material parameters except piezoelectric and spin-orbit coefficients that are taken from Refs. [36] and [37], respectively). The axial electric field \mathcal{E} is used to tune the electron delocalization between QDs, hence the amount of occupation transferred during tunneling, to be the same for all structures. The basis of four lowest-energy states is computed, $\{|1-\rangle, |1+\rangle, |2-\rangle, |2+\rangle\}$ with corresponding energies $E_{1(2)\pm}$, where $|\pm\rangle = (|\downarrow\rangle \pm |\uparrow\rangle)/\sqrt{2}$ are Zeeman eigenstates in the in-plane magnetic field \mathbf{B} ($|\uparrow/\downarrow\rangle$ are spin eigenstates along the z -axis), and the number indicates the QD, in which the electron is mostly localized. The corresponding energy diagram and projections of probability densities in the two orbital states are shown in Fig. 1(b). We shall speak of electron with spin \pm in QDi, referring to the dominant spin and location of a given state.

The acoustic-phonon bath is described with

$$H_{\text{ph}} = \sum_{\mathbf{q}, \lambda} \hbar \omega_{\mathbf{q}, \lambda} b_{\mathbf{q}, \lambda}^\dagger b_{\mathbf{q}, \lambda}$$

TABLE I. Structural and calculated characteristics of selected structures at $T = 0$ K.

Label	r_1 (nm)	c_1	$10^3 \Delta g$	τ_+ (ns)	τ_- (ns)	$10^3 C $
S3	12.5	0.5	94.7	1.778	1.601	7.12
S17	12.5	0.45	36.1	0.782	0.788	40.2
S32	13.4	0.4	5.38	0.807	0.806	232
S35	16.1	0.4	52.8	0.221	0.224	95.2
SX	12.5	0.4112	0.0097	2.043	2.042	499.97

where $b_{\mathbf{q}, \lambda}^\dagger$ creates a λ -branch phonon with wave vector \mathbf{q} , frequency $\omega_{\mathbf{q}, \lambda} = q c_\lambda$, and velocity c_λ . The electron-phonon interaction enters via

$$H_{\text{int}} = \sum_{ij} \sigma_{ij} \int d^3\mathbf{r} \psi_i^\dagger(\mathbf{r}) [H_{\text{B-P}}^{(\text{ph})}(\mathbf{r}) + V_{\text{p}}(\mathbf{r})] \psi_j(\mathbf{r}),$$

where $\sigma_{ij} = |i\rangle\langle j|$, ψ_i is an 8-component pseudo-spinor of the i -th eigenstate envelope functions expressed in the standard $\mathbf{k}\cdot\mathbf{p}$ basis,²⁸ $H_{\text{B-P}}^{(\text{ph})}$ is the Bir-Pikus Hamiltonian evaluated with the phonon-induced strain field $\hat{\epsilon}_{\text{ph}}$ to account for the deformation-potential coupling,^{38,39} $V_{\text{p}}(\mathbf{r}) = i(\hat{d}\hat{\epsilon}_{\text{ph}})_{\parallel}/\epsilon_0\epsilon_r$ is the phonon-induced piezoelectric field potential, and \hat{d} is the third-rank piezoelectric tensor. While various higher-order phonon effects are known,^{40–42} the leading-order contributions present in $H_{\mathbf{k}\cdot\mathbf{p}} + H_{\text{int}}$ (including spin-orbit^{40,43} and shear-strain-induced⁴⁴ admixture mechanisms, phonon-strain-driven: spin-orbit splitting of the electron spectrum and g -factor modification,^{40,43} the acoustic-phonon Pavlov-Firsov coupling,^{45–47} etc.) tend to dominate under typical conditions.^{40,41,44}

Orbital and spin degrees of freedom of the electron undergo dissipative evolution modeled with a non-secular Markovian Redfield equation⁴⁸ for the reduced density matrix,

$$\dot{\rho}(t) = \frac{1}{i\hbar} [H_Z, \rho(t)] + \pi \sum_{ijkl} \left\{ e^{i(\tilde{\omega}_{ij} - \tilde{\omega}_{kl})t} R_{jkl}(\omega_{kl}) \times [\sigma_{kl}\rho(t)\sigma_{ij}^\dagger - \sigma_{ij}^\dagger\sigma_{kl}\rho(t)] + \text{H.c.} \right\}, \quad (1)$$

written in the interaction picture with respect to the orbital energy

$$H_0 = \sum_i \epsilon_i^{(0)} (|i+\rangle\langle i+| + |i-\rangle\langle i-|),$$

but with the Zeeman term

$$H_Z = \frac{1}{2} \mu_B B \sum_i g_i (|i+\rangle\langle i+| - |i-\rangle\langle i-|)$$

kept in the Schrödinger picture. Here, $g_i = \epsilon_i^{(Z)}/\mu_B B$ are effective electron g -factors, $\epsilon_i^{(0)} = (E_{i+} + E_{i-})/2$ and $\epsilon_i^{(Z)} = E_{i+} - E_{i-}$ are the respective orbital and Zeeman energy contributions, $\hbar\omega_{ij} = E_j - E_i$, $\hbar\tilde{\omega}_{ij} = \epsilon_j^{(0)} - \epsilon_i^{(0)}$,

$$R_{ijkl}(\omega) = R_{klij}(\omega) = R_{lkji}^*(\omega) = \frac{1}{\hbar^2} |n(\omega) + 1| \sum_{\mathbf{q}, \lambda} H_{\text{int}}^{(ij)} H_{\text{int}}^{(kl)} \delta(|\omega| - \omega_{\mathbf{q}, \lambda})$$

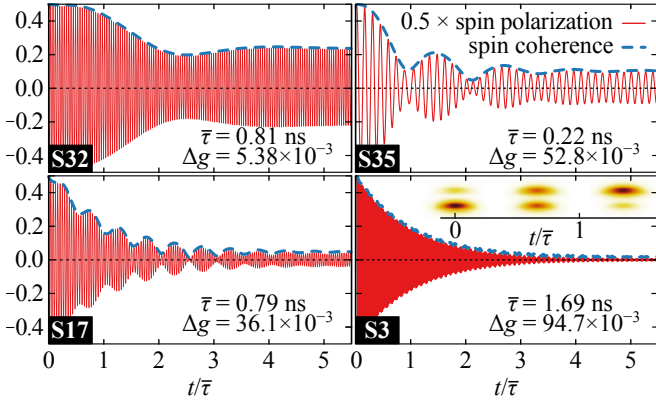


FIG. 2. Evolution of spin polarization (solid red lines) and coherence (dashed blue lines) for chosen structures. Time is given in units of average tunneling time $\bar{\tau}$. Inset: evolution of electron density during tunneling.

are phonon spectral densities,⁴⁹ $H_{\text{int}}^{(ij)} = \langle i|H_{\text{int}}|j\rangle$, and $n(\omega)$ is the Bose distribution. Spin-dependent tunneling rates are determined from the Fermi's golden rule,

$$\Gamma_{\pm} = \frac{1}{\tau_{\pm}} = 2\pi R_{ijji}(\omega_{ji}); \quad (i, j) = (2\pm, 1\pm).$$

We solve Eq. (1) numerically with $\rho(0) = |2\uparrow\rangle\langle 2\uparrow|$, corresponding to optical initialization with a circular polarization, for $B = 5$ T and at $T = 0$ K, unless otherwise stated.

In Fig. 2, we present the evolution of spin polarization $\sum_i (\langle i\uparrow|\rho|i\uparrow\rangle - \langle i\downarrow|\rho|i\downarrow\rangle)$ and coherence $|\sum_i \langle i-|\rho|i+\rangle|$ during tunneling for selected structures differing mainly in the mismatch of Zeeman splittings between QDs, $\Delta_Z = \Delta g \mu_B B$. One may notice damping of spin precession accompanied by a proportional coherence loss, both related to but not uniquely determined by Δ_Z , which suggests that another factor is involved. Importantly, the decoherence takes place once in the course of tunneling, and then the spin coherence becomes constant after a period of several spin-averaged tunneling times $\bar{\tau} = (\tau_+ + \tau_-)/2$.

III. GENERAL THEORY

To relate the above result to the discussed dephasing mechanism, we find the post-tunneling spin coherence within the Weisskopf-Wigner theory of spontaneous emission^{50,51} adapted to the phonon bath and spin-dependent tunneling. Namely, we calculate spin coherence that would remain in the system if the only dephasing originated from the emission of distinguishable phonons.

Spin-preserving tunneling is asymptotically described as

$$(\alpha_+|2+\rangle + \alpha_-|2-\rangle)|\varnothing\rangle \xrightarrow{t \rightarrow \infty} \alpha_+|1+\rangle|\omega_+\rangle + \alpha_-|1-\rangle|\omega_-\rangle, \quad (2)$$

where $|\varnothing\rangle$ is the bath initial state characterized by average phonon numbers $n_{q,\lambda}$. Spin-dependent final states $|\omega_{\pm}\rangle$, corresponding to dissipated energies $\hbar\omega_{\pm} = \Delta \pm \Delta_Z/2$ [see Fig. 1(b)],

are expanded in phonon modes,

$$|\omega_{\pm}\rangle = \sum_{q,\lambda} \frac{1}{\sqrt{n_{q,\lambda} + 1}} c_{q,\lambda}^{(\pm)} b_{q,\lambda}^{\dagger} |\varnothing\rangle; \quad c_{q,\lambda}^{(\pm)} \in \mathbb{C}.$$

The spin-off-diagonal element of the target-QD (QD1) part of the reduced density matrix,

$$\rho(\infty) = \text{Tr}_{\text{ph}}(\mathcal{C}_0|1-\rangle\langle 1+| \otimes |\omega_-\rangle\langle \omega_+| + \dots),$$

where $\mathcal{C}_0 \equiv \alpha_+^* \alpha_-$, embodies the preserved spin coherence,

$$C = \langle 1-|\rho(\infty)|1+\rangle = C_0 \langle \omega_+|\omega_-\rangle = C_0 \sum_{q,\lambda} c_{q,\lambda}^{(+)*} c_{q,\lambda}^{(-)} \quad (3)$$

strictly related to the overlap of bath states $\langle \omega_+|\omega_-\rangle$, which is a measure of their distinguishability.⁵² We calculate the coefficients $c_{q,\lambda}^{(\pm)}$, using H_{int} in the interaction picture and rotating-wave approximation,

$$\mathcal{H}_{\text{int}} = \hbar \sum_{\eta=\pm} |1\eta\rangle\langle 2\eta| \sum_{q,\lambda} g_{q,\lambda}^{(\eta)*} b_{q,\lambda} e^{i(\omega_{\eta} - \omega_{q,\lambda})t} + \text{H.c.},$$

where $g_{q,\lambda}^{(\pm)} = H_{\text{int}}^{(1\pm 2\pm)}/\hbar \equiv g_{q,\lambda}$ for spin-diagonal coupling assumed here. We look for a solution to the Schrödinger equation, $i\hbar|\dot{\Psi}(t)\rangle = \mathcal{H}_{\text{int}}|\Psi(t)\rangle$, in the form (2),

$$|\Psi(t)\rangle = c(t)(\alpha_+|2+\rangle + \alpha_-|2-\rangle) \otimes |\varnothing\rangle + \sum_{\eta=\pm} \alpha_{\eta}|1\eta\rangle \otimes \sum_{q,\lambda} \frac{1}{\sqrt{n_{q,\lambda} + 1}} c_{q,\lambda}^{(\eta)}(t) b_{q,\lambda}^{\dagger} |\varnothing\rangle.$$

This leads to a linear integro-differential equation for $c(t)$,

$$\begin{aligned} \dot{c}(t) &= - \sum_{\eta=\pm} \sum_{q,\lambda} |g_{q,\lambda}|^2 \int_0^t dt' e^{i(\omega_{\eta} - \omega_{q,\lambda})(t-t')} c(t') \\ &= - \sum_{\eta=\pm} \int_{-\infty}^{\infty} d\omega J(\omega) \int_0^t dt' e^{i(\omega_{\eta} - \omega)(t-t')} c(t'), \end{aligned}$$

where

$$J(\omega) = R_{2112}(\omega)|_{T=0\text{K}} = \sum_{q,\lambda} |g_{q,\lambda}|^2 \delta(\omega - \omega_{q,\lambda}).$$

The leading contribution to the time integral comes from the $1/t \sim \tau_{\pm}^{-1}$ -wide vicinity of $\omega = \omega_{\pm}$, where $J(\omega) \approx J(\omega_{\pm}) = \Gamma_{\pm}/2\pi$. Then, integration yields $c(t) = c(0) e^{-2\bar{\Gamma}t}$, where $\bar{\Gamma} = (\Gamma_+ + \Gamma_-)/2$. Next, the solution for $c_{q,\lambda}^{(\pm)}(t)$ is found,

$$c_{q,\lambda}^{(\pm)}(t) = g_{q,\lambda} \frac{1 - e^{i(\omega_{q,\lambda} - \omega_{\pm})t - \Gamma_{\pm}t/2}}{\omega_{q,\lambda} - \omega_{\pm} + i\Gamma_{\pm}/2} \xrightarrow{t \rightarrow \infty} \frac{g_{q,\lambda}}{\omega_{q,\lambda} - \omega_{\pm} + i\Gamma_{\pm}/2},$$

where the limit delivers the asymptotic $c_{q,\lambda}^{(\pm)}$. Inserting the latter into Eq. (3), we finally get

$$C = C_0 \int_{-\infty}^{\infty} \frac{d\omega J(\omega)}{\prod_{\eta=\pm} (\omega - \omega_{\eta} - \eta i\Gamma_{\eta}/2)} \approx \frac{C_0}{1 - i\Delta_Z/\hbar\bar{\Gamma}}, \quad (4)$$

where $C_0 = 1/2$ in our case and the integral is calculated with the residue theorem, assuming that $\Gamma_{\pm} \ll \omega_{\pm}$.

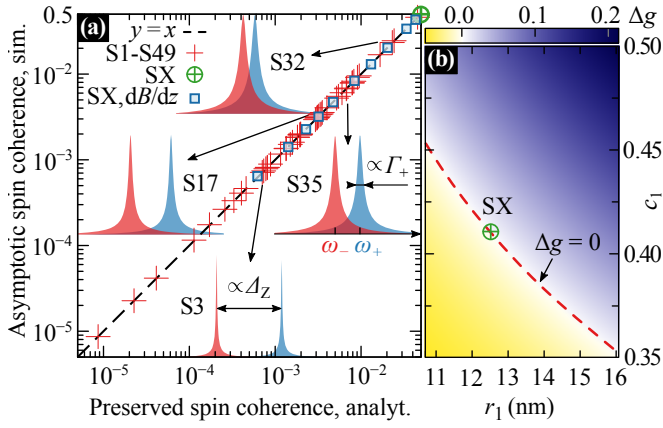


FIG. 3. (a) Spin coherence preserved after tunneling: simulation, Eq. (1), vs. analytical solution, Eq. (4), for structures S1-S49 (+), SX (\oplus) and for SX with a magnetic-field gradient (\square). Insets: spectra of phonon wave packets emitted during tunneling in the two spin states for chosen structures. (b) Interpolated dependence of the g -factor mismatch Δg on QD1 size r_1 and In content c_1 .

According to Eq. (4), faster tunneling is favorable for higher coherence, but it is not a matter of competition between rates of tunneling and decoherence. The dephasing is a one-time process tied to the tunneling and it is not characterized by own rate. Instead, the characteristic parameter is Δ_Z , which is not related directly to any rate and defines the degree of coherence loss, rather than its time scale.

IV. RESULTS AND DEPHASING CONTROL PROTOCOLS

In this Section, we compare the numerical results from Sec. II with those obtained according to the general theory from Sec. III. Then, we propose methods for controlling the degree of dephasing.

In Fig. 3(a), we confront preserved spin coherence \mathcal{C} calculated according to Eq. (4) with post-tunneling values obtained from numerical simulations for 49 structures. The two match perfectly, proving that the discussed dephasing is the dominant spin decoherence channel in the system, apart from possible higher-order phonon couplings beyond our model.⁴² Moreover, by varying the QD1 size and composition within reasonable ranges, one may cover the full range of $|\mathcal{C}|$ values. We propose to use this tunability to design structures of desired properties. While, according to Eq. (4), the preserved coherence is a function of Δ_Z and Γ_{\pm} , these parameters depend on the QD morphology, as well as on external fields. Fig. 3(b) shows the dependence of Δg on the size and composition of QD1, indicating that it varies considerably and changes sign when the morphology is modified within a relatively narrow range of realistic values. The green circles in Figs. 3(a) and 3(b) correspond to an additional structure SX, designed to cancel the mismatch of Zeeman splittings, and hence the dephasing.

Let us note that the effect is expected in any material system: the variation of g -factor with QD size is unavoidable and bulk g -factors^{53,54} for common systems exhibit substan-

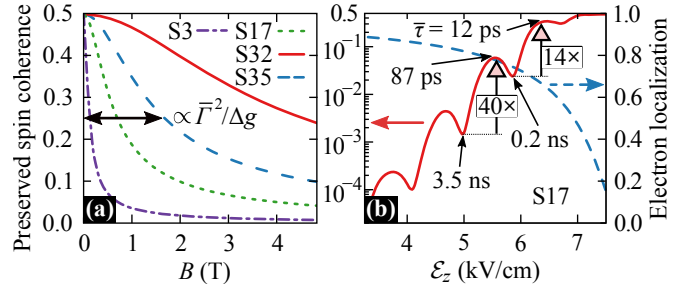


FIG. 4. (a) Dependence of spin coherence preserved after tunneling $|\mathcal{C}|$ on magnetic field B for chosen structures. (b) Dependence of $|\mathcal{C}|$ (solid red line, left axis) and electron localization (dashed blue line, right axis) on axial electric field \mathcal{E}_z . Vertical arrows mark possible coherence gains. Tunneling times are given at local extrema.

tial mismatches, often higher than for InGaAs discussed here. Additionally, $\Delta_Z \neq 0$ may also arise, even for $\Delta g = 0$, due to a magnetic-field gradient. Blue squares in Fig. 3(a) correspond to the structure SX, which has negligible g -factor mismatch, subject to field gradients in the range $0.65 \times 10^{-n/3}$ T/nm, $n = 0, \dots, 9$ (from left to right). The resulting dephasing is equivalent to that caused by Δg . For the highest simulated gradient (orders of magnitude higher than ~ 0.1 -1 mT/nm met in current nanodevices⁵⁵), a 6% deviation from Eq. (4) occurs, resulting from enhanced spin-flips in the high local field.

A practical control protocol should rely on external fields applied to the sample rather than manufacturing conditions. Obviously, since dephasing is due to the mismatch of Zeeman splittings, it can be eliminated by reducing the magnitude of the magnetic field. The dependence of $|\mathcal{C}|$ on the latter is plotted for chosen structures in Fig. 4(a), showing a Lorentzian-like shape of width $\propto \bar{\Gamma}^2/\Delta g$. Thus, a fast tunneling regime (represented by S32) may be used to widen the range of B for reasonably coherent tunneling. On the other hand, slow tunneling allows one to toggle coherence on and off with small changes in low magnetic field, e.g., $|\mathcal{C}|$ from 0.035 at $B = 1$ T to 0.5 at $B = 0$ T for structure S3. In principle, a gradient $dB_x/dz \approx -2B_0\Delta g/D(g_1 + g_2)$ could be used to cancel Δ_Z , although this may be hardly feasible.

Another way of controlling spin dephasing is to use oscillations in tunneling rates with transition energy (period $\propto D^{-1}$)^{56,57} that may be tuned with an axial electric field. This changes also the degree of electron localization, up to now kept fixed. Both these dependencies are plotted in Fig. 4(b). We find that decoherence can be controlled within a range of values extending over many orders of magnitude, while keeping the electron localized and with reasonable tunneling times. Thus, a feasible, on-demand control of dephasing is possible.

V. CUMULATIVE DEPHASING AT FINITE TEMPERATURE

While in the previous sections we dealt with the $T = 0$ K limit, here we study the additional dephasing that arises at finite temperatures.

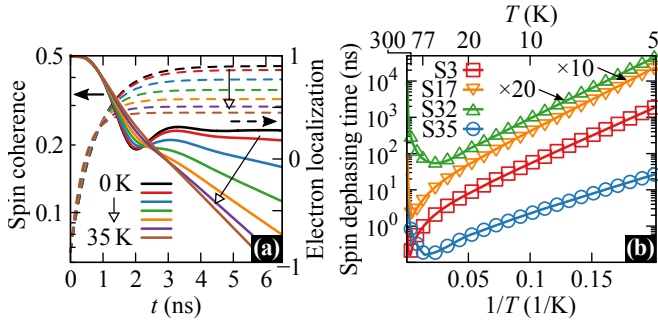


FIG. 5. (a) Evolution of spin coherence (solid lines, left axis) and electron localization (dashed lines, right axis) for structure S32 at various temperatures. (b) Arrhenius plot of post-tunneling spin dephasing times from simulations (symbols) and calculated with Eq. (6) (lines) for selected structures.

Saturation of spin coherence in Fig. 2 results from the fact that tunneling at $T = 0$ K is irreversible, hence the dephasing takes place once. At $T > 0$ K, thermally activated back-tunneling enables a continuous dephasing process, accompanying the repeated virtual tunneling between the QDs. For a better insight, we analyze the Master equation (1) analytically in the interaction picture with respect to H_Z . Labels are here changed for brevity: $\{1-, 1+, 2-, 2+\} \rightarrow \{\bar{1}, 1, \bar{2}, 2\}$. To account only for the studied mechanism, we neglect all spin-off-diagonal couplings by setting $R_{ijkl} = 0$ if either of pairs (i, j) , (k, l) is spin-mismatched and assume couplings to be spin-invariant, *i.e.*, $R_{ij12} = R_{ij\bar{1}\bar{2}}$, *etc.* This decouples equations for spin coherence,

$$\langle \bar{2} | \dot{\rho} | 2 \rangle \simeq -\pi [R(\omega_+) + R(\omega_-)] \langle \bar{2} | \rho | 2 \rangle + \pi [R(-\omega_+) + R(-\omega_-)] \langle \bar{1} | \rho | 1 \rangle e^{-i\omega_Z t}, \quad (5a)$$

$$\langle \bar{1} | \dot{\rho} | 1 \rangle \simeq -\langle \bar{2} | \dot{\rho} | 2 \rangle e^{i\omega_Z t}, \quad (5b)$$

where $R(\omega) \equiv R_{2112}(\omega)$, and $\omega_Z \equiv \Delta_Z/\hbar = \omega_+ - \omega_-$. At $T = 0$ K, $R(-\omega_{\pm})$ vanish and only the first term in Eq. (5a) is left, describing an exponential outflow of coherence from QD2 at the rate $\pi[R(\omega_+) + R(\omega_-)] = \bar{\Gamma}$, *i.e.*, exactly during tunneling. The associated inflow to QD1, according to Eq. (5b), is affected by a phase factor that oscillates with a frequency equal to the mismatch of Larmor precession frequencies ω_Z . The solution for the target-QD spin coherence,

$$\mathcal{C}(t) \simeq \langle \bar{1} | \rho | 1 \rangle|_{T=0\text{K}} = \mathcal{C}_0 \frac{1 - e^{i\omega_Z t - \bar{\Gamma}t}}{1 - i\omega_Z/\bar{\Gamma}} \xrightarrow{t \rightarrow \infty} \mathcal{C},$$

reproduces Eq. (4) derived within the spontaneous emission theory. The terms that arise in Eqs. (5) at $T > 0$ K describe the transfer of spin coherence in the opposite direction via thermally activated back-tunneling at a rate

$$\Gamma_v \equiv \frac{1}{2} (e^{-\hbar\omega_+/kT} \Gamma_+ + e^{-\hbar\omega_-/kT} \Gamma_-) \simeq \bar{\Gamma} e^{-\Delta/kT}.$$

This leads to the solution with a long-time exponential decay of spin coherence at the rate given by

$$2\Gamma_d = \bar{\Gamma} + \Gamma_v - \text{Re} \sqrt{(\bar{\Gamma} + \Gamma_v)^2 + 2i\omega_Z(\Gamma_v - \bar{\Gamma}) - \omega_Z^2}. \quad (6)$$

Thus, at $T > 0$ K, after the dephasing during tunneling, the remaining coherence undergoes exponential decay of similar origin. Temperature-driven emergence of the latter in the equilibrated part of evolution is visible in Fig. 5(a), where the simulated spin coherence is presented along with electron localization. The dependence of corresponding dephasing times on temperature is shown in Fig. 5(b), where values extracted from numerical simulations (symbols) are compared to Γ_d calculated according to Eq. (6) (lines). The agreement indicates that, up to room temperature, the considered dephasing channel dominates over other processes included in numerical simulations but deliberately neglected in the analytical solution for Γ_d . Interestingly, a non-monotonic behavior is present due to the interplay between the temperature-driven rise of accumulative dephasing and the overall decrease of phonon distinguishability with rising tunneling rates.

While the one-time dephasing applies to carriers that actually tunnel, the exponential decoherence at $T > 0$ K may affect also stationary spins in tunnel-coupled structures. The dephasing time depends nontrivially on system parameters and widely varies among simulated structures. For $B = 5$ T it may be as short as ~ 10 ns at $T = 5$ K and ~ 0.1 ns at $T = 77$ K. Hence, it may vary from comparable to a few orders of magnitude shorter than homogeneous dephasing times due to hyperfine interaction^{58–60} (μs range) and, under certain conditions, may even surpass the inhomogeneous dephasing ($\sim 2\text{--}20$ ns^{58–60}). The other relevant source of spin perturbation, the charge noise, has been recently found to lead to slower spin pure relaxation.⁶¹ Thus, the discussed effect may be the one to limit spin coherence time in tunnel-coupled structures.

VI. CONCLUSIONS

We have presented a prediction of a spin pure dephasing channel in a spin-preserving electron orbital relaxation in a magnetic field between states with unequal Zeeman splittings. The dephasing originates from distinguishability of reservoir excitations induced by the mismatch of energies dissipated during transitions in the two spin states, and hence the resulting leakage of information on the spin superposition to the environment. The mechanism is thus general and of fundamental nature analogous to measuring the position of a particle in double-slit experiments. Our theoretical analysis of reservoir state distinguishability within the theory of spontaneous emission showed that the effect depends on the difference of Zeeman splittings and relaxation rates. These parameters define the spectral overlap of phonon wave packets emitted during relaxation in the two spin states. Additionally, we have presented a detailed quantitative analysis of spin dephasing for the case of spin-preserving tunneling between self-assembled QDs via a realistic multi-band $\mathbf{k} \cdot \mathbf{p}$ modeling and simulations using a non-secular Markovian master equation. In this case, the effect is expected in virtually any material system. We have shown that the considered mechanism is the only leading-order phonon-related spin perturbation relevant in the double QD system and that it may limit spin coherence time in tunnel-coupled structures at cryogenic temperatures. Finally, we have

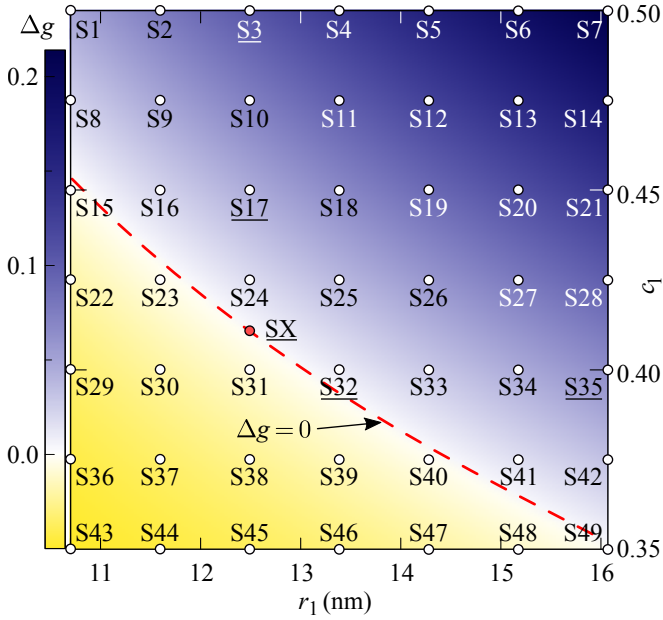


FIG. A1. Interpolated dependence of the g -factor mismatch Δg on QD1 size r_1 and In content c_1 . Parameters (size and composition of QD1) of structures are represented by position of dots with their labels, underlined for structures used as exemplary in the paper.

proposed ways of controlling spin decoherence both at the stage of sample manufacturing via the size and composition of QDs, and on demand, by tuning of external fields. The latter promises a feasible method of a real-time control over spin decoherence in a range that covers many orders of magnitude.

ACKNOWLEDGMENTS

We acknowledge support from the Polish National Science Centre by Grants No. 2014/13/B/ST3/04603 (K.G., P.M.) and No. 2011/02/A/ST3/00152 (M.G.). We would also like to thank M. Syperek for an inspiring discussion. Numerical calculations have been carried out using resources provided by Wroclaw Centre for Networking and Supercomputing (<http://wcss.pl>), Grant No. 203.

Appendix: Details of numerically modeled structures

In this Appendix, we describe the set of numerically modeled DQD structures used in the paper, give their structural and calculated characteristics, as well as describe the procedure used for interpolation of Δg values.

In total, we modeled 50 DQD structures of realistically varying morphology. Those labeled S1-S49 differ in the QD1 base radius r_1 and indium composition c_1 [see Fig. 1(a)] and form a 7×7 axis-wise regular grid in the r_1 - c_1 plane. The additional structure SX is designed to simulate a dephasing-free system with approximately equal g -factors in the two QDs. Characteristics of all modeled structures are presented in Table AI,

TABLE AI. Characteristics of modeled structures: QD1 radius r_1 and In content c_1 , calculated g -factor mismatch Δg , transition energies $\hbar\omega_{\pm}$ and tunneling times τ_{\pm} for electrons in the two spin states, as well as spin coherence preserved after tunneling $|C|$ at $T = 0$ K and $B = 5$ T. Structures used as exemplary in the paper are highlighted.

	r_1 (nm)	c_1	Δg $\times 10^3$	$\hbar\omega_+$ (meV)	$\hbar\omega_-$ (meV)	τ_+ (ns)	τ_- (ns)	$ C $ $\times 10^3$
S1	10.7	0.5	41.0	4.41	4.40	10.8	10.5	2.61
S2	11.6	0.5	67.2	3.61	3.60	0.851	0.886	19.5
S3	12.5	0.5	94.7	3.02	2.99	1.78	1.60	7.12
S4	13.4	0.5	123	2.52	2.49	0.527	0.636	15.9
S5	14.3	0.5	153	2.13	2.08	0.226	0.237	32.1
S6	15.2	0.5	183	1.81	1.75	0.329	0.301	19.8
S7	16.1	0.5	213	1.52	1.46	0.601	0.607	8.87
S8	10.7	0.475	17.8	4.70	4.69	5.53	5.50	11.6
S9	11.6	0.475	40.1	3.88	3.87	2.05	2.17	13.4
S10	12.5	0.475	63.7	3.21	3.20	0.921	0.892	19.7
S11	13.4	0.475	88.6	2.70	2.67	1.51	1.80	7.78
S12	14.3	0.475	114	2.28	2.24	0.269	0.294	35.4
S13	15.2	0.475	140	1.96	1.92	0.243	0.241	33.4
S14	16.1	0.475	167	1.65	1.60	0.48	0.431	15.0
S15	10.7	0.45	-2.21	4.97	4.97	6.15	6.14	82.6
S16	11.6	0.45	16.2	4.09	4.09	8.49	8.80	8.13
S17	12.5	0.45	36.1	3.43	3.42	0.782	0.788	40.2
S18	13.4	0.45	57.2	2.88	2.86	2.77	2.65	7.36
S19	14.3	0.45	79.2	2.44	2.41	0.445	0.496	30.5
S20	15.2	0.45	101	1.99	1.96	0.214	0.214	52.2
S21	16.1	0.45	125	1.77	1.74	0.320	0.301	29.4
S22	10.7	0.425	-19.1	5.24	5.24	13.1	12.8	4.59
S23	11.6	0.425	-4.39	4.37	4.37	14.2	14.2	18.2
S24	12.5	0.425	11.8	3.66	3.66	1.19	1.20	79.3
S25	13.4	0.425	29.4	3.06	3.05	1.26	1.23	31.0
S26	14.3	0.425	48.0	2.61	2.59	1.16	1.28	19.4
S27	15.2	0.425	67.0	2.20	2.18	0.245	0.256	67.3
S28	16.1	0.425	86.8	1.90	1.88	0.239	0.236	54.8
S29	10.7	0.4	-32.9	5.56	5.57	86.9	80.9	0.413
S30	11.6	0.4	-21.6	4.62	4.63	6.49	6.54	8.08
S31	12.5	0.4	-8.83	3.90	3.90	3.79	3.72	34.3
S32	13.4	0.4	5.38	3.30	3.30	0.807	0.806	232
S33	14.3	0.4	20.5	2.80	2.79	3.05	3.04	18.2
S34	15.2	0.4	36.3	2.39	2.38	0.444	0.467	68.2
S35	16.1	0.4	52.8	2.05	2.03	0.221	0.224	95.2
S36	10.7	0.375	-43.4	5.85	5.87	295	311	0.0865
S37	11.6	0.375	-35.5	4.92	4.93	8.00	7.82	4.05
S38	12.5	0.375	-25.9	4.15	4.16	25.8	25.3	1.72
S39	13.4	0.375	-14.9	3.50	3.51	0.967	0.957	78.5
S40	14.3	0.375	-2.91	2.99	2.99	1.39	1.40	244
S41	15.2	0.375	9.76	2.57	2.57	1.25	1.27	91.1
S42	16.1	0.375	23.2	2.21	2.20	0.275	0.280	167
S43	10.7	0.35	-50.8	6.17	6.18	97.5	99.9	0.227
S44	11.6	0.35	-46.0	5.20	5.21	22.6	21.1	1.13
S45	12.5	0.35	-39.4	4.44	4.45	8.62	8.89	3.30
S46	13.4	0.35	-31.4	3.77	3.78	2.75	2.60	13.6
S47	14.3	0.35	-22.3	3.21	3.21	0.835	0.837	60.5
S48	15.2	0.35	-12.6	2.75	2.76	2.89	2.89	31.3
S49	16.1	0.35	-2.07	2.36	2.36	0.466	0.464	460
SX	12.5	0.4112	0.0097	3.72	3.72	2.04	2.04	499.97

where also calculated g -factor mismatch Δg , tunneling times τ_{\pm} and transition energies $\hbar\omega_{\pm}$ as well as spin coherence preserved after tunneling, $|C|$, at $T = 0$ K and $B = 5$ K are given. In Fig. A1, the structures are represented by positions of dots with respective labels in the r_1 - c_1 plane, where also the interpolated dependence of Δg is plotted as a color map. The interpolation was done with a surface of the first and second order in r_1 and c_1 , respectively. This is justified, as we expect a close to linear dependence of electron g -factor on a uniform QD size change^{62,63} and terms up to second order in the In concentration, presumably inherited after quadratic corrections to the interpolation of the bulk g -factor between GaAs and InAs, which is commonly referred to as *bowing*.⁶⁴

- 1 R. P. Feynman, R. B. Leighton, and M. Sands, *The Feynman Lectures on Physics, Vol. I: The New Millennium Edition: Mainly Mechanics, Radiation, and Heat* (Basic Books, 2010).
- 2 P. Sonnentag and F. Hasselbach, *Phys. Rev. Lett.* **98**, 200402 (2007).
- 3 P. Roulleau, F. Portier, P. Roche, A. Cavanna, G. Faini, U. Gennser, and D. Mailly, *Phys. Rev. Lett.* **102**, 236802 (2009).
- 4 S. Frabboni, G. C. Gazzadi, and G. Pozzi, *Appl. Phys. Lett.* **97**, 263101 (2010).
- 5 M. Richter, M. Kunitski, M. Schöffler, T. Jahnke, L. P. H. Schmidt, M. Li, Y. Liu, and R. Dörner, *Phys. Rev. Lett.* **114**, 143001 (2015).
- 6 H. Yanagisawa, M. Ciappina, C. Hafner, J. Schötz, J. Osterwalder, and M. F. Kling, *Sci. Rep.* **7**, 12661 (2017).
- 7 T. Korn, *Phys. Rep.* **494**, 415 (2010).
- 8 I. Žutić, J. Fabian, and S. Das Sarma, *Rev. Mod. Phys.* **76**, 323 (2004).
- 9 D. Awschalom, D. Loss, and N. Samarth, *Semiconductor spintronics and quantum computation* (Springer, 2002).
- 10 R. Hanson, L. P. Kouwenhoven, J. R. Petta, S. Tarucha, and L. M. K. Vandersypen, *Rev. Mod. Phys.* **79**, 1217 (2007).
- 11 A. Galindo and M. A. Martín-Delgado, *Rev. Mod. Phys.* **74**, 347 (2002).
- 12 N. Gisin, G. Ribordy, W. Tittel, and H. Zbinden, *Rev. Mod. Phys.* **74**, 145 (2002).
- 13 M. H. Mikkelsen, J. Berezovsky, N. G. Stoltz, L. A. Coldren, and D. D. Awschalom, *Nature Physics* **3**, 770 (2007).
- 14 A. J. Ramsay, S. J. Boyle, R. S. Kolodka, J. B. B. Oliveira, J. Skiba-Szymanska, H. Y. Liu, M. Hopkinson, A. M. Fox, and M. S. Skolnick, *Phys. Rev. Lett.* **100**, 197401 (2008).
- 15 T. M. Godden, S. J. Boyle, A. J. Ramsay, A. M. Fox, and M. S. Skolnick, *Appl. Phys. Lett.* **97**, 061113 (2010).
- 16 T. M. Godden, J. H. Quilter, A. J. Ramsay, Y. Wu, P. Brereton, I. J. Luxmoore, J. Puebla, A. M. Fox, and M. S. Skolnick, *Phys. Rev. B* **85**, 155310 (2012).
- 17 T. M. Godden, J. H. Quilter, A. J. Ramsay, Y. Wu, P. Brereton, S. J. Boyle, I. J. Luxmoore, J. Puebla-Nunez, A. M. Fox, and M. S. Skolnick, *Phys. Rev. Lett.* **108**, 017402 (2012).
- 18 R. P. Feynman, *Int. J. Theor. Phys.* **21**, 467 (1982).
- 19 D. Loss and D. P. DiVincenzo, *Phys. Rev. A* **57**, 120 (1998).
- 20 M. Krzykowski, M. Gawelczyk, and P. Machnikowski, *Acta Phys. Pol. A* **130**, 1165 (2016).
- 21 M. Kroutvar, Y. Ducommun, D. Heiss, M. Bichler, D. Schuh, G. Abstreiter, and J. J. Finley, *Nature* **432**, 81 (2004).
- 22 M. Kugler, K. Korzekwa, P. Machnikowski, C. Gradl, S. Furthmeier, M. Griesbeck, M. Hirmer, D. Schuh, W. Wegscheider, T. Kuhn, C. Schüller, and T. Korn, *Phys. Rev. B* **84**, 085327 (2011).
- 23 K. Müller, A. Bechtold, C. Ruppert, C. Hautmann, J. S. Wildmann, T. Kaldewey, M. Bichler, H. J. Krenner, G. Abstreiter, M. Betz, and J. J. Finley, *Phys. Rev. B* **85**, 241306 (2012).
- 24 M. A. Migliorato, A. G. Cullis, M. Fearn, and J. H. Jefferson, *Phys. Rev. B* **65**, 115316 (2002).
- 25 V. Jovanov, T. Eissfeller, S. Kapfinger, E. C. Clark, F. Klotz, M. Bichler, J. G. Keizer, P. M. Koenraad, M. S. Brandt, G. Abstreiter, and J. J. Finley, *Phys. Rev. B* **85**, 165433 (2012).
- 26 M. G. Burt, *J. Phys. Condens. Matter* **4**, 6651 (1992).
- 27 B. A. Foreman, *Phys. Rev. B* **48**, 4964 (1993).
- 28 T. B. Bahder, *Phys. Rev. B* **41**, 11992 (1990).
- 29 T. Andlauer, R. Morschl, and P. Vogl, *Phys. Rev. B* **78**, 075317 (2008).
- 30 G. Bir and G. Pikus, *Symmetry and Strain-induced Effects in Semiconductors*, A Halsted Press book (Wiley, 1974).
- 31 C. Pryor, *Phys. Rev. B* **57**, 7190 (1998).
- 32 G. Bester, X. Wu, D. Vanderbilt, and A. Zunger, *Phys. Rev. Lett.* **96**, 187602 (2006).
- 33 S. Schulz, M. A. Caro, E. P. O'Reilly, and O. Marquardt, *Phys. Rev. B* **84**, 125312 (2011).
- 34 G. Tse, J. Pal, U. Monteverde, R. Garg, V. Haxha, M. A. Migliorato, and S. Tomić, *J. Appl. Phys.* **114**, 073515 (2013).
- 35 K. Gawarecki, P. Machnikowski, and T. Kuhn, *Phys. Rev. B* **90**, 085437 (2014).
- 36 M. A. Caro, S. Schulz, and E. P. O'Reilly, *Phys. Rev. B* **91**, 075203 (2015).
- 37 R. Winkler, *Spin-Orbit Coupling Effects in Two-Dimensional Electron and Hole Systems* (Springer, Berlin, Heidelberg, 2003).
- 38 L. M. Woods, T. L. Reinecke, and R. Kotlyar, *Phys. Rev. B* **69**, 125330 (2004).
- 39 K. Roszak, V. M. Axt, T. Kuhn, and P. Machnikowski, *Phys. Rev. B* **76**, 195324 (2007).
- 40 A. V. Khaetskii and Y. V. Nazarov, *Phys. Rev. B* **64**, 125316 (2001).
- 41 L. M. Woods, T. L. Reinecke, and Y. Lyanda-Geller, *Phys. Rev. B* **66**, 161318 (2002).
- 42 P. San-Jose, G. Zarand, A. Shnirman, and G. Schön, *Phys. Rev. Lett.* **97**, 076803 (2006).
- 43 A. V. Khaetskii and Y. V. Nazarov, *Phys. Rev. B* **61**, 12639 (2000).
- 44 A. Mielnik-Pyszczorski, K. Gawarecki, M. Gawelczyk, and P. Machnikowski, *Phys. Rev. B* **97**, 245313 (2018).
- 45 A. Alcalde, Q. Fanyao, and G. Marques, *Phys. E* **20**, 228 (2004).
- 46 C. L. Romano, G. E. Marques, L. Sanz, and A. M. Alcalde, *Phys. Rev. B* **77**, 033301 (2008).
- 47 Z.-W. Wang and S.-S. Li, *Solid State Commun.* **152**, 1098 (2012).
- 48 F. Breuer, H. and Petruccione, *The Theory of Open Quantum Systems* (Oxford University Press, 2007).
- 49 K. Roszak, A. Grodecka, P. Machnikowski, and T. Kuhn, *Phys. Rev. B* **71**, 195333 (2005).
- 50 V. Weisskopf and E. Wigner, *Z. Physik* **63**, 54 (1930).
- 51 M. O. Scully and M. S. Zubairy, *Quantum Optics* (Cambridge University Press, 1997).
- 52 D. Dieks, *Phys. Lett. A* **126**, 303 (1988).
- 53 L. M. Roth, B. Lax, and S. Zwerdling, *Phys. Rev.* **114**, 90 (1959).
- 54 M. Willatzen, M. Cardona, and N. E. Christensen, *Phys. Rev. B* **51**, 17992 (1995).
- 55 J. Yoneda, T. Otsuka, T. Takakura, M. Pioro-Ladrière, R. Brunner, H. Lu, T. Nakajima, T. Obata, A. Noiri, C. J. Palmström, A. C. Gossard, and S. Tarucha, *Appl. Phys. Express* **8**, 084401 (2015).
- 56 K. C. Wijesundara, J. E. Rolon, S. E. Ulloa, A. S. Bracker, D. Gammon, and E. A. Stinaff, *Phys. Rev. B* **84**, 081404 (2011).
- 57 K. Gawarecki, M. Pochwała, A. Grodecka-Grad, and P. Machnikowski, *Phys. Rev. B* **81**, 245312 (2010).
- 58 J. Petta, A. Johnson, J. Taylor, E. Laird, A. Yacoby, M. Lukin, C. Marcus, M. Hanson, and A. Gossard, *Phys. E* **35**, 251 (2006).
- 59 A. Bechtold, D. Rauch, F. Li, T. Simmet, P.-L. Ardelit, A. Regler, K. Müller, N. A. Sinitsyn, and J. J. Finley, *Nat. Phys.* **11**, 1005 (2015).
- 60 R. Stockill, C. L. Gall, C. Matthiesen, L. Huthmacher, E. Clarke, M. Hugues, and M. Atatüre, *Nat. Commun.* **7**, 12745 (2016).
- 61 P. Huang and X. Hu, *Phys. Rev. B* **89**, 195302 (2014).
- 62 T. Nakaoka, T. Saito, J. Tatebayashi, and Y. Arakawa, *Phys. Rev. B* **70**, 235337 (2004).
- 63 J. van Bree, A. Y. Silov, P. M. Koenraad, M. E. Flatté, and C. E. Pryor, *Phys. Rev. B* **85**, 165323 (2012).
- 64 I. Vurgaftman, J. R. Meyer, and L. R. Ram-Mohan, *J. Appl. Phys.* **89**, 5815 (2001).